Lawrence Berkeley National Laboratory
Lawrence Berkeley National Laboratory

Title

HIGH SPATIAL RESOLUTION MWPC FOR MEDICAL IMAGING WITH POSITRON EMITTERS

Permalink

https://escholarship.org/uc/item/6sp2q79k

Author

Del Guerra, A.

Publication Date

1982-03-01

eScholarship.org Powered by the California Digital Library
University of California

LBL--14044

DE82 014477

High-Spatial-Resolution MWPC for Medical Imaging with Positron Emitters+

A. Del Guerra,* V. Perez-Mendez, G. Schwartz, B. Sleaford

Lawrence Berkeley Laboratory, University of California, Berkeley, Berkeley, California 94720 U.S.A.

Abstract

The performance of a 15 x 15 cm^2 MultiWire Proportional Chamber (MWPC) with lead glass tube converter is presented. A standard Argon-Methane (70-30) gas mixture has been used at various pressures between 1.0 and 2.0 atm. For 511 keV γ-rays incident almost perpendicular onto a 1.0 cm thick lead glass tube converter, a detection efficiency of 4.5%, a time resolution of 130 ns (FWHM) and a spatial resolution of 1.3 mm (FWHM) has been obtained at 2 atm. Fast delay lines, capacitively coupled to the cathodes, standard integrated amplifiers and comparator electronics have been adopted for the position read-out. The use of fast delay lines (specific delay 8 ns/cm) ensures a high rate capability. A multiplanar positron camera is proposed, made of six MWPC modules arranged to form the lateral surface of a hexagonal prism. Each module (50 x 50 cm^2) will have a 2 cm thick converter on both sides of the chamber and will be operating at 2 atm. The expected performance is presented and compared with that of a recent multi-ring BGO camera, and is shown to be superior in spatial resolution and comparable in event rate at a considerably lower cost.

+This work was supported by the Director, Office of Energy Research, Office of High Energy and Nuclear Physics, Division of High Energy Physics of the US Department of Energy under Contract No. DE-AC03-76SF00098

*On leave of absence from: Istituto di Fisica dell'Universita', Piazza Torricelli, 2, I-56100 Pisa, Italy

DISCLAIMER

1. INTRODUCTION

A well known figure of merit parameter of multiplanar positron cameras is ϵ^2/τ , where ϵ is the efficiency of one module and τ is the FWHM of the time resolution. In a previous paper [1] we have presented the imaging performance of a two-plane MWPC positron camera, consisting of two MWPC modules (48 x 48 cm^2 active area) equipped with converters made of lead corrugated banded strips[2] In the case of a dense drift space MWPC positron camera τ is the transit time of the primary ionization electrons within the converter. Since then we have developed lead glass tube converters[3] with a higher surface to volume ratio in order to increase the efficiency of the chamber. Several gas mixtures have also been investigated [4] in order to obtain a higher electron drift velocity within the converter tube, thus improving the time resolution.

In this paper the performance of a 15 x 15 cm^2 MWPC test module with a 1 cm thick lead glass tube converter is reported for a standard Argon-Methane (70-30) gas mixture at various pressures, ranging from 1.0 to 2.0 atm. Experimental results obtained at 1.2 atm have been partially presented in a previous paper [5]. The description of the chamber and of the converter is given in Section 2; the experimental measurements of efficiency, time and spatial resolution are presented in Section 3 and discussed in Section 4. In the last section a new design - a six module MWPC positron camera - is proposed and its expected performance is discussed.

2. EXPERIMENTAL APPARATUS

We have built some 50 x 50 cm^2 MWPC modules, but, for convenience, we have extensively tested a smaller module, consisting of a MWPC (15 x 15 cm^2 active area) and a 1 cm thick lead glass converter, both contained in an aluminum box filled with the Argon-Methane (70-30) mixture.

2.1 - The Chamber

The MWPC is of conventional construction (fig 1): the anode plane is made of 20 μm stainless steel wires spaced 3 mm apart and connected to a positive high voltage V_a, through a load protection

resistor; the two cathode planes consist of 100 μm stainless steel wires spaced 2 mm apart and coupled through 220 kΩ resistors to a common bus bar. The anode cathode gap is 5 mm. The direction of the wires in the cathode planes are arranged at 90° relative to each other in order to allow both x and y localization. The cathodes are kept at a positive voltage V_c relative to ground in order to drift the electrons out of the lead converter.

2.2 - The Converter

The detection of 511 keV gamma rays with a MWPC requires the use of a high density, high Z converter with large surface to volume ratio. Several designs have been implemented: insulated tungsten wire meshes[6], corrugated lead banded strips [2] and perforated metal plates [7,8]. We have developed a converter made of glass capillaries of high lead content (80% PbO by weight, glass density 6.2 g/cm^3), fused to form honeycomb matrices. The converter has been treated by an acidic leaching process and then by an H_2 reduction process to provide uniform surface resistivity on the inner walls of the glass tubes. Electric fields higher than 1000 V/cm can be applied with a constant gradient within the tubes. Details of converter construction and treatment have been reported elsewhere [3,9]. A typical converter is shown in Fig. 2.

Following the gamma interaction within the converter, the Compton- or photo-electron has a finite range depending on its energy. If it reaches the gas region within the tube, a number of primary ionization eletrons are produced. A voltage difference, V_{conv}, applied between the ends of the tube then drifts the electrons along the electric field lines towards the cathode and into the avalanche region of the chamber.

2.3 - Delay Line Read-Out

Position read-out is done by means of electromagnetic delay lines, capacitively coupled to the cathode plane wires [10,11]. For each co-ordinate the signal from one end of the delay line is used as the START and that from the other end as the STOP of a Time to Digital Converter. The time information is directly related to

the co-ordinate position. Because of the large dynamic variation of the signals - both in amplitude and in rise time - Zero Crossing and Constant Fraction Discriminators are not particularly suitable for the delay line signals, especially if saturation of the amplifiers is possible. The time resolution of a leading-edge discriminator, on the other hand, may be severely impaired by time jitter of the signal. We have chosen comparator electronics and fast printed-circuit delay lines[12]. No appreciable distortion of the signal is measured along the line; any timing error introduced by jitter will be the same at each end and will cancel. The main properties of the delay line used are listed in Table 1.

Table 1

Main properties of the delay line

Type	Printed circuit
Length	20.0 cm
Width	3.81 cm
Thickness	0.16 cm
Characteristics Impedance	145 Ω
DC-Resistance	18 Ω
Specific delay	8 ns
Rise time	8 ns
Total Delay/Rise Time	20:1

2.4 - Experimental Set-Up

Figure 3 shows the experimental set-up. A positron emitting ^{68}Ga source is placed between a NaI scintillator and the MWPC. The position of the source relative to the NaI detector is such that a very small solid angle is subtended by the source at the converter plane ($\Delta\Theta \sim 7°$), thus avoiding any edge effects. A small mylar window (100 μm thick) allows the use of an external ^{55}Fe source (5.9 keV X-rays) for calibration purposes.

A schematic drawing of the electronics is shown in Fig. 4. The efficiency of the MWPC is calculated from the coincidence of the NaI

signal with the MWPC anode signal. The acceptance energy window of the NaI discriminator is set to a narrow band around the 511 keV photopeak for background rejection. The output signal from the MWPC anode is amplified 220 times by a fast amplifier (rise time 1.5 ns) and fed to a discriminator. For convenience a Constant Fraction Discriminator was used in most of the measurements. A 260 ns NIM pulse from the NaI discriminator and a 20 ns NIM pulse from the CFD are then fed into a majority logic coincidence unit. The efficiency of the MWPC is given by

$$(1) \qquad \varepsilon = \frac{C - C_{acc}}{S_{NaI} - S_{NaI)\ no\ source}}$$

where C is the coincidence rate between the NaI scintillator and the MWPC, C_{acc} is the accidental coincidence rate, S_{NaI} is the single rate of the NaI scintillator and $S_{NaI)no\ source}$ is the single rate when the ^{68}Ga source has been removed.

The output from the coincidence is used both as a coincidence gate for the delay line signals and as the STOP of a Time to Digital Converter (Lecroy 3001 qVt, in t-mode), the START of which is given by the NaI discriminator. Fast integrated amplifiers (LA733, Gain = 10-400, rise time = 2.5 - 10.5 ns) and comparator electronics (AM 685) are used to handle the delay line signals. Additional majority logic coincidence units measure the relative efficiency of the delay lines with respect to the anode. A TDC (Lecroy 3001 qVt, in t-mode) is used for spatial resolution measurements for the x- and y-coordinates.

The experimental set-up is such that the three characteristic parameters (efficiency, time, and spatial resolution) can be measured simultaneously.

3. EXPERIMENTAL RESULTS

In a previous paper [4], we have shown the results of efficiency measurements and electron transit time studies for various gas mixtures and converter tube diameters. The measurements reported in this section always refer to a 1 cm thick converter

(inner diameter 0.91 mm, outer diameter 1.10 mm), and an Argon-Methane (70-30) gas mixture at various pressures from 1.0 to 2.0 atm. Preliminary results at 1.2 atm have been already reported[5].

3.1 - Efficiency

The efficiency of the module has been measured as a function of the anode CFD threshold at various pressures. The results have been corrected for γ absorption in the aluminum cover.

The operational voltages and the typical anode response to 5.9 keV X-rays and the module efficiency at a CFD threshold of 30 mV are listed in Table 2. The cathode and the converter voltage values in Table 2 maximize the electron drift velocity for each E/p[13]. The anode voltage at each pressure is chosen to give the maximum avalanche gain compatible with a very low single rate for the chamber with no source. An upper limit of $\sim$0.5 Hz/wire has been chosen at a CFD threshold of 30 mV. This single rate is of the same order of magnitude of the expected counting rate from cosmic rays ($\sim$1/min/cm^2/ster). The amplitude of the 5.9 keV X-rays, directly measured into 50Ω termination, increases with pressure from 4.0 to 20 mV.

Table 2

MWPC Operational Voltages and Anode Response at Various Pressures

Pressure (atm)	1.0	1.2	1.8	2.0
V_{eff} ($\equiv V_a - V_c$) (V)	2850	3150	4000	4250
V_c (V)	330	400	600	670
V_{conv} (V)	-330	-400	-600	-670
5.9 keV X-ray amplitude into 50 Ω termination (mV)	4	10	18	20
511 keV γ's efficiency x 10^2 (anode CFD threshold at 30 mV)	3.0	4.0	4.4	4.5

The efficiency results are shown in Fig. 5 (solid lines). The pressures and the effective anode voltage ($V_{eff} = V_a - V_c$) are also indicated. The dashed line represents the preliminary efficiency results at 1.2 atm, obtained with a higher V_{eff}, and with a chamber background 10 times higher. Figure 6 shows the module efficiency variation with the cathode (Fig. 6a) and converter voltage (Fig. 6b). For both measurements the value of V_{eff} was

kept constant at 3350 V, the gas pressure at 1.2 atm and the CFD threshold at 30 mV. The arrows indicate the voltage settings which give the maximum electron drift velocity. Both the measurements were taken with the standard 280 ns coincidence gate.

3.2 Time Resolution

The transit time of the primary ionization electrons within the glass tubes largely determines the time resolution of the system. If the voltages are chosen to maximize the electron drift velocity, a time resolution of 130 ns (FWHM) is obtained at all pressures. A typical time spectrum is shown in Fig 7a. Fig. 7b shows the dependence of the FWHM of the time resolution upon the converter voltage, at 1.2 atm, V_{eff} = 3350 V and V_c = -400 V. The experimental values obtained are in good agreement with predictions from the electron drift velocity data of reference (13).

3.3 - Spatial Resolution at 1.2 Atm

An extensive study has been done of the spatial resolution at 1.2 atm, with the following voltage settings: V_{eff} = 3350 V, V_c = 400 V, V_{conv} = -400 V, and CFD threshold = 30 mV.

Typical spectra for uniform illumination of the converter are shown in Fig. 8: the top spectrum refers to the x-delay line (i.e. the one perpendicular to the anode plane wires); the anode wire structure is clearly visible. The bottom spectrum applies to the y-coordinate (the y-delay line is parallel to the anode plane wires) and reveals the cathode wire structure, which spatially modulates the electrons drifted from the converter into the chamber. This modulation increases with increasing cathode - converter voltage difference and disappears when the cathode is grounded. The presence of the anode (3 mm spacing) and cathode (2 mm spacing) wire structures in the spectra offers a precise method for calibrating the specific delay of the delay lines. Similar spectra, taken under different illumination conditions of the converter, are shown in Fig. 9a and 9b for the x- and y- coordinate, respectively.

The spatial resolution along the y-direction has been measured by collimating the ^{68}Ga source with a 2" thick lead variable

slit. To enhance the signal to noise ratio, only the coincidence (NaI-MWPC) events were accepted. The threshold chosen for the comparators corresponds to an input threshold of ~180 μV for the μA733 amplifier. In this condition the relative efficiency of the delay line was ~70%. The results are shown in Fig. 10, as a function of the slit opening. Typical spectra are shown in Fig. 11a and 11b for various slit widths.

The efficiency of the delay line depends on the threshold applied to the comparators. To keep the maximum efficiency the threshold must be set at a very low level, comparable with the noise of the system. As the comparator threshold is raised the efficiency diminishes, but the spatial resolution improves. At a relative efficiency of 100%, 2.8 mm (FWHM) has been measured and at 70%, ~2.3 mm. As the limit of the spatial resolution is reached (0.9 mm FWHM, i.e. the tube diameter), the relative efficiency has dropped to 30%.

The measured spatial resolution along the x - coordinate is ~3 mm (FWHM), due to the 3 mm spacing of the anode wire.

3 4 - Spatial Resolution at 2.0 Atm

The spatial resolution has been measured at the various pressures as listed in Table 2. At high pressure the gain increases (see Table 2) and a higher threshold may be applied to the comparator without any efficiency loss, thus giving a better signal/noise ratio and improving the spatial resolution.

A typical spatial distribution spectrum is shown in Fig. 12a for the x-coordinate and a 2.0 mm slit. The two peaks correspond to the anode wires 3 mm apart. A similar distribution for the y-coordinate and for a 750 μm slit is shown in Fig. 12b. The FWHM of the spatial distribution spectrum is 1.6 mm. Note the considerable improvement over the same spectrum taken at lower pressure (Fig. 11a). Once the contribution due to the slit-opening has been accounted for, a spatial resolution of 1.3 mm (FWHM) is obtained at 2 atm.

4. DISCUSSION

At atmospheric pressure 20-50 mV amplitude anode signals from a ^{55}Fe source have been observed in proportional counters with

thick anode wires (40-100 μm) for various gas mixtures[14-20]. A limited Geiger regime (or self-quenching streamer mode) has been hypothesized. In pressurized chambers high amplitude pulses have been also observed for thinner wires[21,22]. We think that the amplitude increase observed in the ^{55}Fe signal in going from 1.0 to 2.0 atm is due to the same phenomena.

The amplitude spectrum of electrons produced by the 511 keV interaction inside the converter is continuous. Thus it is conceivable that upon increasing the avalanche gain more and more events will have an amplitude above the CFD threshold. Furthermore, raising the pressure enhances the probability of primary ionization electrons being produced within the converter. This combined effect is evident in the efficiency curves presented in Fig. 5; for instance, for a CFD threshold of 30 mV the module efficiency rises from 3.0×10^{-2} to 4.0×10^{-2}, going from 1.0 to 1.2 atm. Similarly, increasing of V_{eff} from 3150 to 3350 V at 1.2 atm produces an efficiency of 4.3×10^{-2}. However, if the gain is high enough so that any small amount of primary ionization gives rise to a signal well above threshold, any further pressure increase will modify the efficiency only slightly. In fact, in going from 1.8 to 2.0 atm, for the same 30 mV threshold, the efficiency changes only from 4.4 to 4.5×10^{-2}. An increase in the avalanche gain and in the probability of primary ionization produces an overall shift of the spectrum towards higher amplitudes. Then, even if the absolute efficiency does not vary much, the longer efficiency plateau obtained at higher pressure allows much more stable operation (i.e. farther away from the electronic noise level) and a much better spatial resolution. As described in section 3, in fact, the spatial resolution (FWHM) along the y-coordinate improves from 2.7 mm (1.2 atm), to 1.8 mm (1.8 atm), to 1.3 mm (2.0 atm).

From the efficiency curves shown in Fig. 5 it is also clear that the maximum efficiency has been reached for this type of converter and this gas mixture. Similar converters developed at CERN[8] and made of perforated metal plates were shown to have basically the

same performance [5]. Any further improvement can only be achieved by increasing the surface to volume ratio. New converters with smaller diameter tubes are now being assembled.

The spatial resolution obtained at 2.0 atm (1.3 mm along the y-coordinate) is more than adequate for a positron camera because of the intrinsic position spread, which is caused by both the finite range of the β's and the deviation from colinearity of the two annihilation quanta.

5. THE PROPOSED POSITRON CAMERA

A schematic drawing of the camera is shown in Fig. 15. Six modules, 50 x 50 cm^2 each, are arranged to form the lateral surface of a hexagonal prism. Each module consists of a standard MWPC chamber (2 mm spacing for both anode and cathode planes), at 2 atm, with 2 cm thick converters on both sides (chambers pressurized to 2 atm create no engineering problems, nor will they be serious safety hazards in a hospital environment). Fast delay lines (8 ns/cm) will be used, as will a fast gas mixture, such as 69% Ar + 20%CH_4 +10% CF_4 +1% C_2H_2[4]. The expected efficiency is 15%, with a time resolution of 200 ns (FWHM). From the relation [1]

$$(2) \qquad \varepsilon^2/\tau = \frac{8(\text{true coincidences})^2}{\text{accidentals}}$$

assuming the rate of true coincidences and accidentals to be equal, we obtain a true coincidence rate of 14000 c/sec per module pair.

In table 3 the performance of the proposed camera is compared with that of the previous two-plane positron camera[1] and with that of the multi-ring NIH - Neuro PET [23], the latter specifically designed as a high spatial resolution camera for brain imaging. While the efficiency and time resolution of the MWPC solution are still less favorable than those of the BGO camera, the spatial resolution is better. It has been shown [24] that the spatial resolution compensates for poorer efficiency when

Table 3

Positron Camera Specifications and Performance

	Previous work[1]	NIH-Neuro PET[23]	This paper
Type	Dense drift space MWPC (Corrugated lead banded strip converter)	Multi-ring of BGO scintillator (4 rings)	Dense drift space MWPC (lead glass tube converter)
Camera inner diameter	48 cm	38 cm	85 cm
Number of elements	2	4 x 128	6
Active area of each element	48 x 48 cm^2	8.5 x 20 mm^2	45 x 45 cm^2
Time Resolution (FWHM)	300 ns	20 ns	200 ns
Efficiency of each element	0.058	0.70(+)	0.15
Point response function in air	7.0 mm	4.6 mm	1.5(++) mm
Operating counting rate (true coincidences = accidentals)	500 c/s	144000 c/s	84000 c/s
Multislice capability	YES	YES	YES
Number of simultaneous slices for a 15x15x15 cm^3 object	15 (~1 cm slice)	4 (~1 cm slice)	50 (~3 mm slice)

(+) In high sensitivity mode

(++) Estimated using a 2 mm (FWHM) spatial resolution along the x-coordinate and 1.3 mm along the y-coordinate

reconstructing an image. In addition, the MWPC has a three-dimensional capability, with a voxel (volume element) determined by the detector resolution. As many as fifty 3 mm slices may be simultaneously produced for a 15 x 15 x 15 cm^3 object.

6. CONCLUDING REMARKS

We have studied the performance of a dense drift space MWPC test module for 511 keV γ-rays. We have measured the three characteristic parameters: efficiency (4.5%), time resolution (130 ns FWHM) and spatial resolution (1.3 mm FWHM for the y-coordinate).

A six module MWPC positron camera has been proposed as a high spatial resolution camera for medical imaging with positron emitters. Its expected performance has been compared with that of a recent multiring BGO camera and is shown to be very competitive.

Further work is now in progress to simulate the performance of such a camera for a point-like source embedded in a 20 cm diameter water phantom. The EGS code[25] will be used and the Monte Carlo data will be reconstructed using limited angle algorithms[26]. The results of the simulation and the reconstructed images will be presented in a forthcoming paper[27].

The progress in electronics technology and the increased knowledge of gas properties has now rendered the MWPC camera very attractive, not only for its low cost and simplicity of construction, but also because of the large solid angle coverage, the high spatial resolution, and its intrinsic fully three-dimensional (multislice) capability.

REFERENCES

1. V. Perez-Mendez, C.B. Lim, D. Ortendahl, R. Semper, A. Cheng, P. Chu, R. Hattner, L. Kaufman and D.C. Price, Nucl. Instr. and Meth., 156 (1978) 33.
2. D. Chu, K.C. Tam, V. Perez-Mendez, C.B. Lim, D. Lambert and S.N. Kaplan, IEEE Trans. Nucl. Sci., NS-23 (1976) 634.
3. G.K. Lum, M.I. Green, V. Perez-Mendez and K.C. Tam, IEEE Trans. Nucl. Sci., NS-27 (1980) 157.
4. G.K. Lum, V. Perez-Mendez and B. Sleaford, IEEE Trans. Nucl. Sci., NS-28 (1981) 821.

5. A. Del Guerra, C.B. Lim, G.K. Lum, D. Ortendahl and V. Perez-Mendez, Lawrence Berkeley Laboratory, LBL-14043, submitted to IEEE Trans. Med. Imag., (1982).

6. J. Votruba, Ceskoslovenska Akademie Ved., Praha, private communication (1979). R. Lanza, MIT, private communication (1980).

7. A.P. Jeavons, Nucl. Instr. and Meth., 156 (1978) 41.

8. A. Jeavons, K. Kull, B. Lindberg, G. Lee, D. Townsend, P. Frey and A. Donath, Nucl. Instr. and Meth., 176 (1980) 89.

9. G.K. Lum, D. Anderberg, M.I. Green, P. Henrickson and V. Perez-Mendez, in Proc. 25th American Scientific Glass-blowers Society Symposium, Albany, N.Y., (June 1980).

10. R. Grove, K. Lee, V. Perez-Mendez and J. Sperinde, Nucl. Instr. and Meth., 89 (1970) 257.

11. R. Grove, I. Ko, B. Leskovar and V. Perez-Mendez, Nucl. Instr. and Meth., 99 (1972) 381. R. Grove, V. Perez-Mendez and J. Sperinde, Nucl. Instr. and Meth., 106 (1973) 407.

12. P. Lecomte, V. Perez-Mendez and G. Stoker, Nucl. Instr. and Meth., 153 (1978) 551.

13. B. Jean-Marie, V. Lepeltier and D. L'Hote, Nucl. Instr. and Meth., 159 (1979) 213.

14. G. Charpak, D. Rahm and H. Steiner, Nucl. Instr. and Meth., 80 (1970) 13 (Section 11).

15. S. Brehin, A. Diamant Berger, G. Marel, G. Tarte, R. Turlay, G. Charpak and F. Sauli, Nucl. Instr. and Meth., 123 (1975) 225.

16. C. Battistoni, E. Iarocci, G. Nicoletti and L. Trasatti, Nucl. Instr. and Meth., 152 (1978) 423.

17. G.D. Alekseev, D.M. Khazins and V.V. Kruglov, Lett. Nuovo Cim., 25 (1979) 157.

18. G.D. Alekseev, N.A. Kalinina, V.V. Karpukhin, D.M. Khazins and V.V. Kruglov, Nucl. Instr. and Meth., 177 (1980) 385.

19. M. Atac, A.V. Tollestrup and D. Potter, Fermilab Report, FN-329 (July 1981), and IEEE Nucl. Sci., NS-29 Vol. 1 (February 1982) 388.

20. T.A. Mulera and V. Perez-Mendez, Lawrence Berkeley Laboratory, LBL-14003, (April 1982), and to be submitted to Nucl. Instr. and Meth.

21. S. Behrends and A.C. Melissinos, Nucl. Instr. and Meth., 188 (1981) 521.

22. A.R. Forouhi, B. Sleaford, V. Perez-Mendez, D. de Fontaine and J. Fodor, Lawrence Berkeley Laboratory, LBL-12587 (April 1981), and IEEE Trans. Nucl. Sci., NS-29 Vol 1 (February 1982) 275.

23. R.A. Brooks, V.J. Sank, W.S. Friauf, S.B. Leighton, H.E. Cascio and G. Di Chiro, IEEE Trans. Biom. Eng., BME-28 (1981) 158.

24. M.E. Phelps, S.C. Huang, E.J. Hoffman, D. Plummer, and R. Carson to be published in J. Comp. Ass. Tom. (1982).

25. R.L. Ford and W.R. Nelson, Stanford Linear Accelerator Center Report, SLAC-210, (June 1978).

26. K.C. Tam and V. Perez-Mendez, J. Opt. Soc. Am., 71 (1981) 582.

27. V. Perez-Mendez, A. Del Guerra, W.R. Nelson, and K.C. Tam, Lawrence Berkeley Laboratory, LBL-14114 (1982) in preparation.

FIGURE CAPTIONS

1. Test chamber with the converter at the bottom separated from the cathode plane by a 5 mm spacing (top). Plane view of the chamber showing the orientation of the cathode planes with the delay lines coupled to them; the anode wires are indicated by dashed lines (bottom).
2. Typical lead glass tube converters. The right one has been H_2 reduced.
3. Schematic diagram of the experimental set-up (Figure not to scale).
4. Schematic diagram of pulse-processing electronics.
5. Efficiency of the module as a function of the anode discriminator threshold at various pressures.
6. Efficiency of the module as a function of cathode voltage (a), and converter voltage (b), with constant V_{eff}, at 1.2 atm.
7. (a) Typical time distribution spectrum as obtained from the coincidence with the NaI scintillator. The FWHM of the distribution is 130 ns (Hor. scale=50 ns/div). The START of the 280 ns coincidence gate is also shown. (b) Time resolution (FWHM) as a function of the converter voltage at 1.2 atm.
8. Typical spatial distributions for uniform illumination of the converter. The top spectrum refers to the x-delay line and the bottom one to the y-delay line. Events counted are "MWPC single" events.
9. (a) Typical spatial distribution along the x-coordinate with limited illumination of the converter, showing the solid angle subtended by the convert r (note anode wire structure). The horizontal scale is 5.0 ns/div. (b) Spatial distribu-

tion with a 750 μm slit illumination of the converter measured along the y-coordinate (Hor. scale=2.0 ns/div). Events counted are "MWPC single" events.

10. Spatial resolution (FWHM) along the y-coordinate as a function of the slit width at 1.2 atm.

11. Spatial distribution spectra along the y-coordinate at 1.2 atm for various slit widths (Hor. scale = 5.0 ns/div): (a) 1500 μm slit; (b) 750 μm slit (left) and 250 μm slit (right), separated by 1 cm. Events counted here are coincidence events.

12. Spatial distribution spectra at 2.0 atm (Hor. scale= 5.0 ns/div): (a) x-coordinate, 2.0 mm slit (note anode wire structure); (b) y-coordinate, 750 μm slit.

13. Proposed Positron Camera made of six modules arranged to form a hexagonal prism.

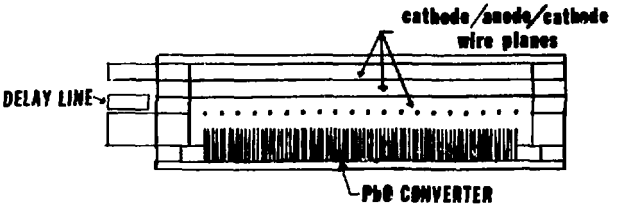
cathode/anode/cathode
wire planes
DELAY LINE
Pb CONVERTER

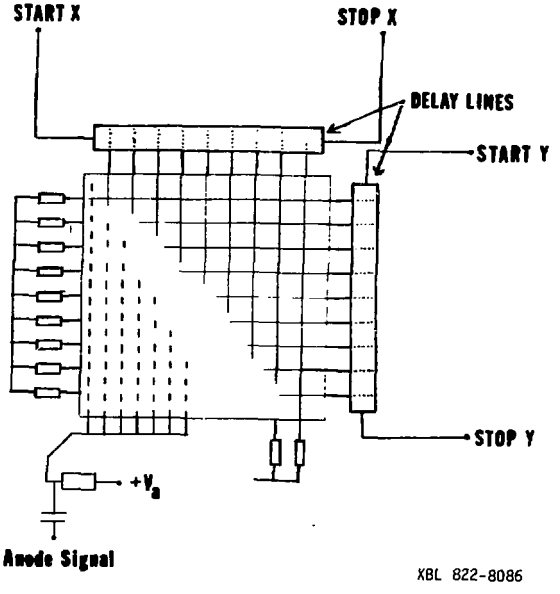
START X
STOP X
DELAY LINES
START Y
STOP Y
+V_a
Anode Signal
XBL 822-8086

F I G. 1

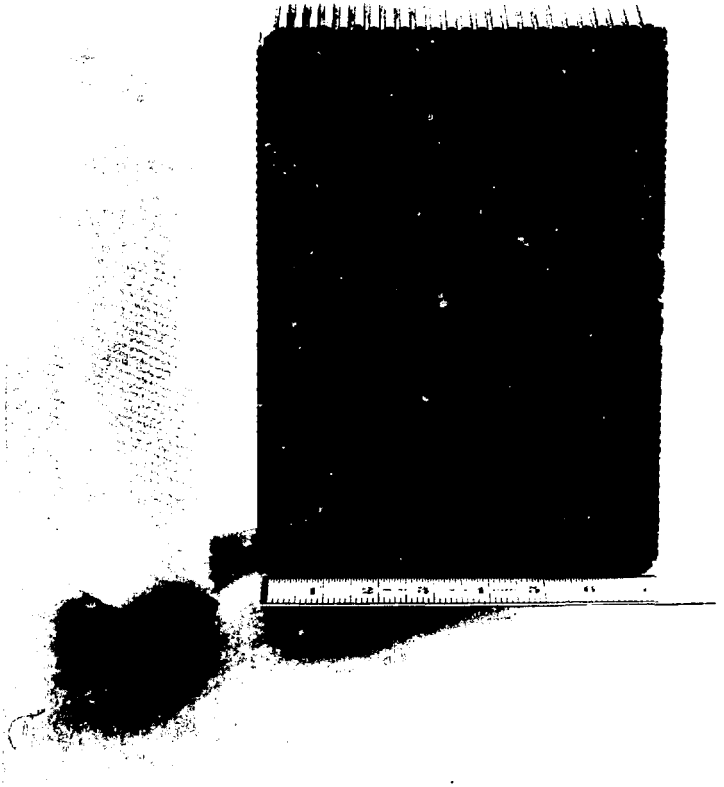

CBL 790-13578

F I G. 2

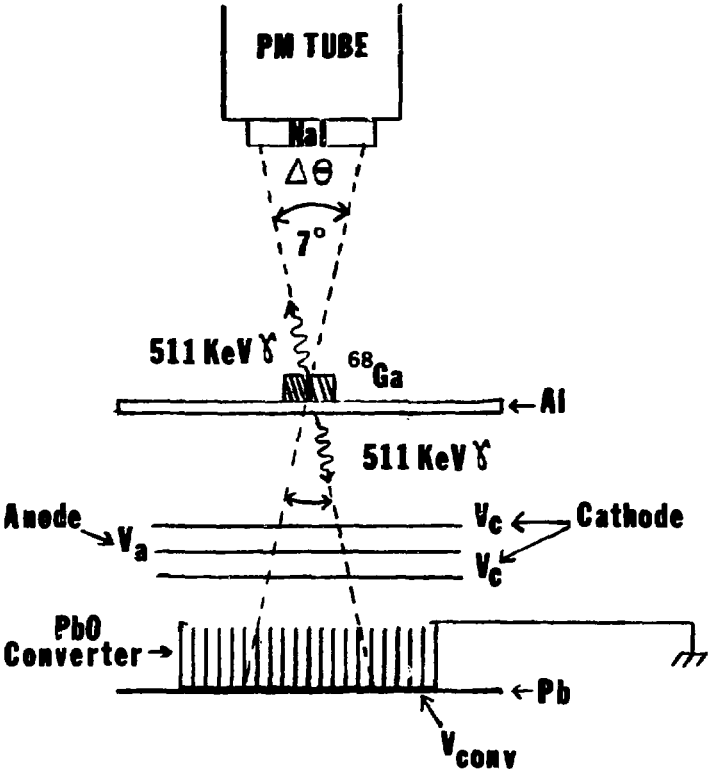

XBL 822-8087

F I G. 3

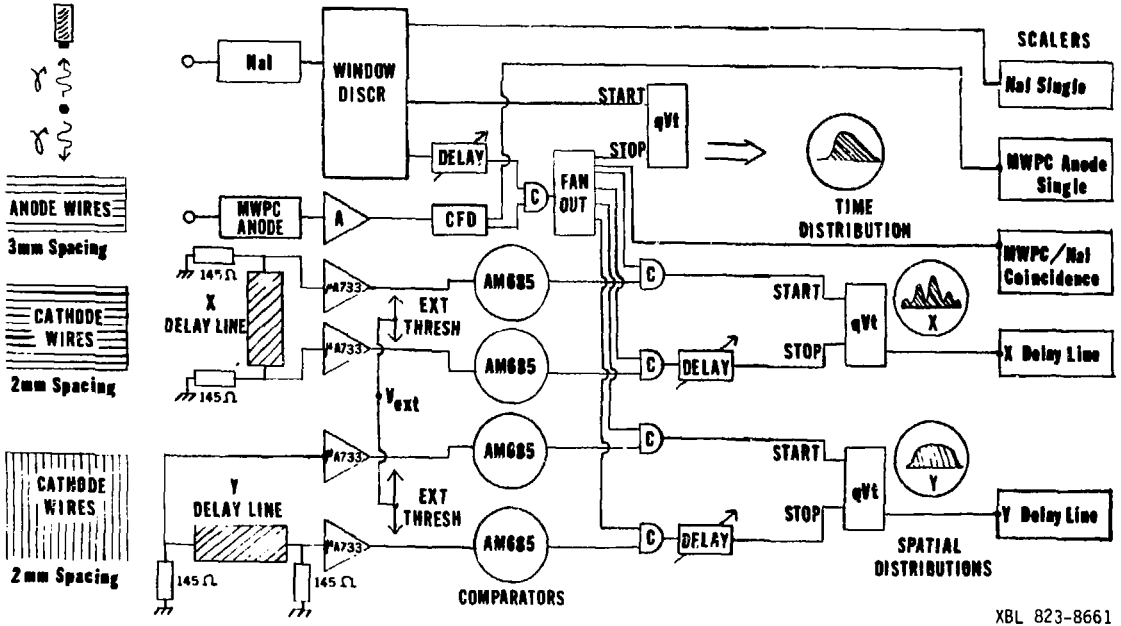
ANODE WIRES
3mm Spacing
CATHODE WIRES
2mm Spacing
CATHODE WIRES
2mm Spacing
NaI
WINDOW DISCR
DELAY
CFD
MWPC ANODE
A
FAN OUT
C
START
STOP
qVt
TIME DISTRIBUTION
SCALERS
NaI Single
MWPC Anode Single
MWPC/NaI Coincidence
X Delay Line
Y Delay Line
145Ω
X DELAY LINE
Y DELAY LINE
A733
EXT THRESH
V_{ext}
AM685
COMPARATORS
X
Y
SPATIAL DISTRIBUTIONS
XBL 823-8661

F I G. 4

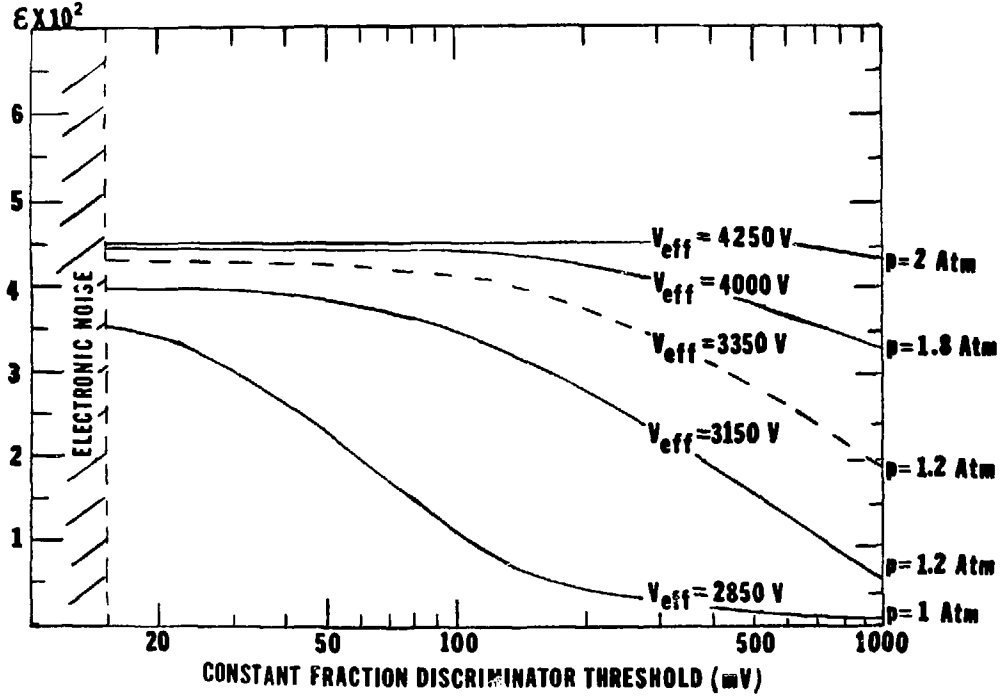

XBL 823-8660

F I G. 5

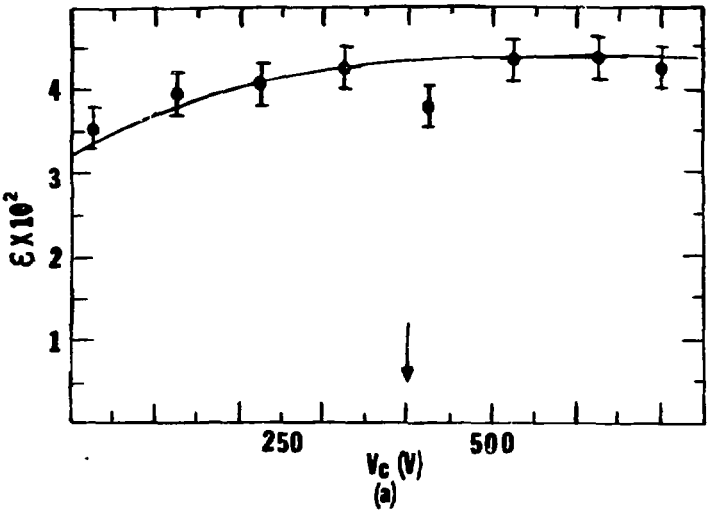

(a)

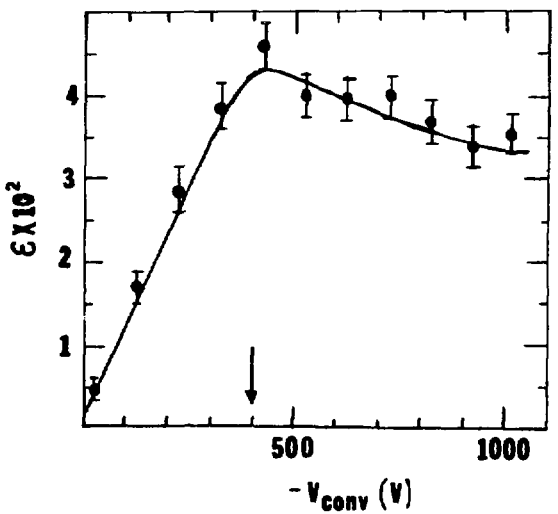

(b)

XBL 823-8659

F I G. 6

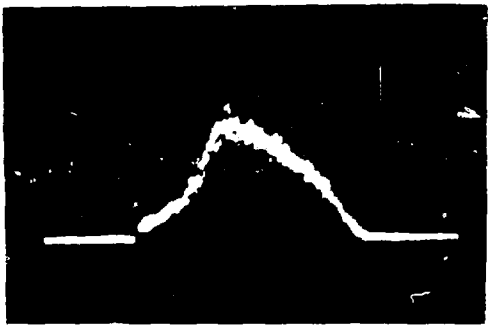

(a)

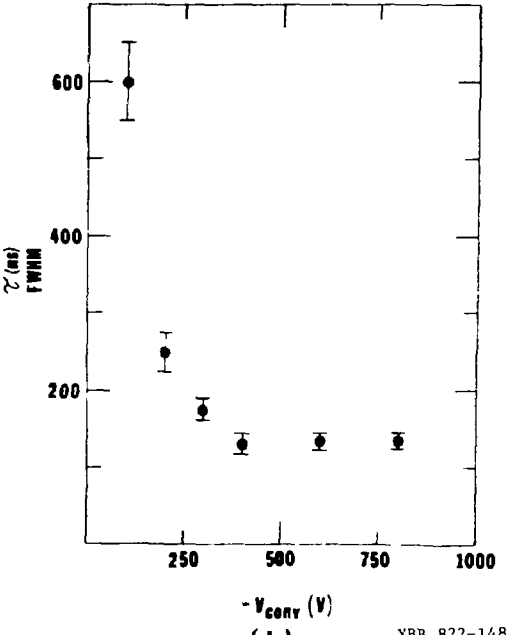

(b)

XBB 822-1481A

F I G. 7

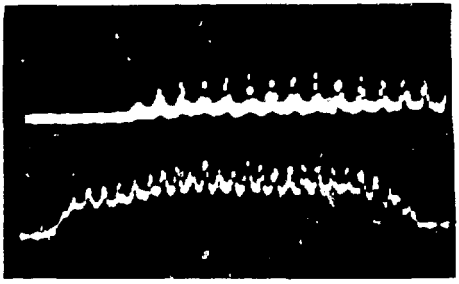

F I G. 8

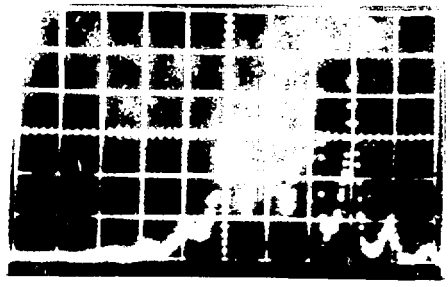

(a)

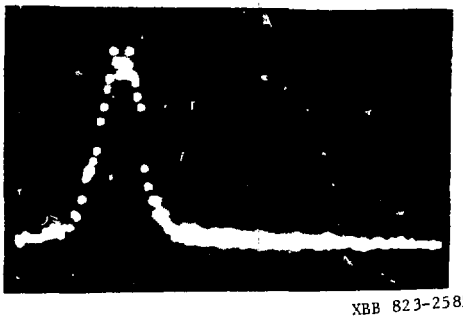

(b)

XBB 823-2585

F I G. 9

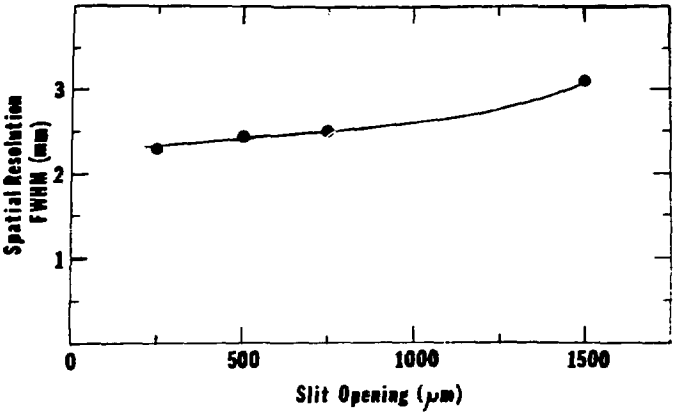

F I G. 10

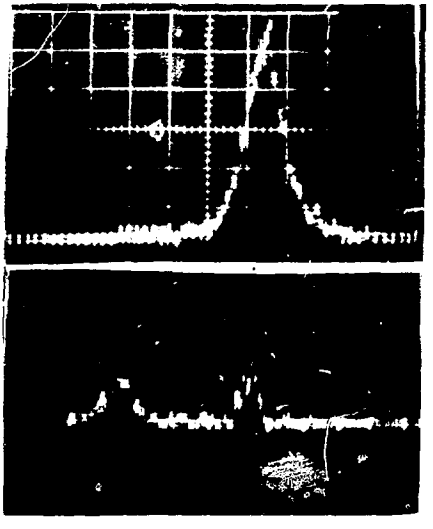

XBB 823-2584

F I G. 11

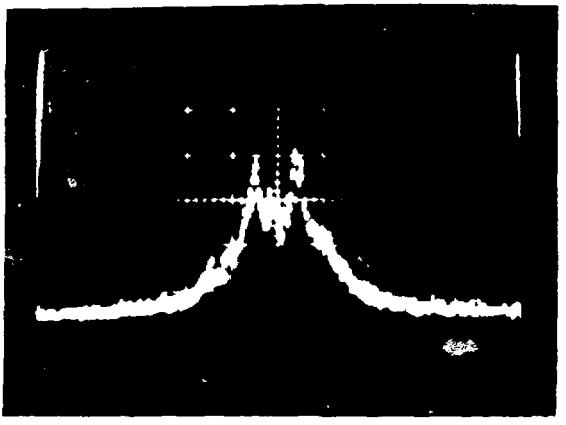

(a)

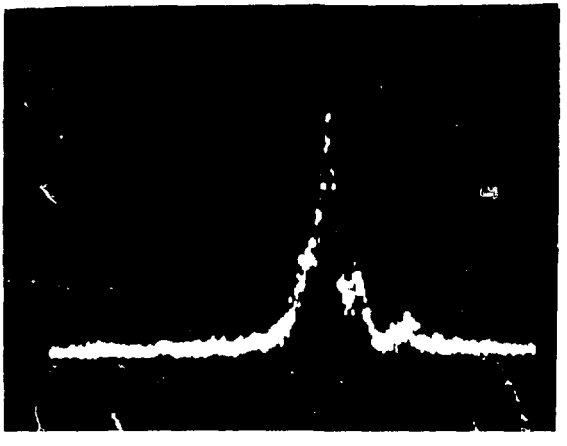

XBB 823-2583

(b)

F I G. 12

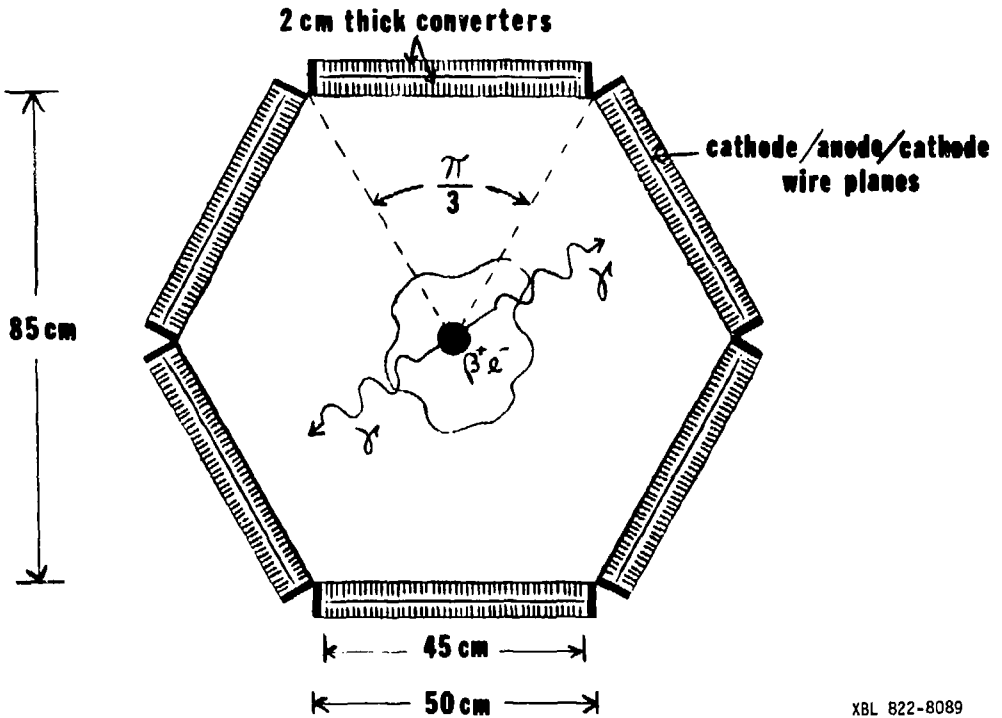
2 cm thick converters
cathode/anode/cathode
wire planes
π/3
85 cm
45 cm
50 cm
XBL 822-8089

F I G. 13